



Effects of norms on general Hookean solids for their isotropic counterparts

Tomasz Danek^a · Andrea Noseworthy^b · Michael A. Slawinski^b

Communicated by Len Bos

Abstract

It is common to assume that a Hookean solid is isotropic. For a generally anisotropic elasticity tensor, it is possible to obtain its isotropic counterparts. Such a counterpart is obtained in accordance with a given norm. Herein, we examine the effect of three norms: the Frobenius 36-component norm, the Frobenius 21-component norm and the operator norm on a general Hookean solid. We find that both Frobenius norms result in similar isotropic counterparts, and the operator norm results in a counterpart with a slightly larger discrepancy. The reason for this discrepancy is rooted in the very definition of that norm, which is distinct from the Frobenius norms and which consists of the largest eigenvalue of the elasticity tensor. If we constrain the elasticity tensor to values expected for modelling physical materials, the three norms result in similar isotropic counterparts of a generally anisotropic tensor. To examine this important case and without loss of generality, we illustrate the isotropic counterparts by commencing from a transversely isotropic tensor obtained from a generally anisotropic one. Also, together with the three norms, we consider the L_2 slowness-curve fit. Upon this study, we infer that—for modelling physical materials—the isotropic counterparts are quite similar to each other, at least, sufficiently so that—for values obtained from empirical studies, such as seismic measurements—the differences among norms are within the range of expected measurement errors.

1 Introduction

The symmetry class of a Hookean solid is a property defined within its elasticity tensor. Such a solid, which is a mathematical entity, might serve as an analogy—in the Platonic sense of mathematical physics—for physical properties of a given material. The inference of properties of a physical material requires the interpretation of an elasticity tensor. Among these properties are its symmetries. In particular, it is useful to compute an isotropic counterpart of the obtained tensor, which might be sufficiently accurate for the modelling of materials, while offering a mathematical convenience. Furthermore, such a result can serve as a starting model for more detailed study, especially if anisotropy does not significantly affect the wave propagation (e.g., Eken et al. [1]). Regardless of the motivation, it is necessary to decide on an appropriate norm to compute such a counterpart. An insight into such a decision is the crux of this paper.

An examination of several norms to obtain an isotropic counterpart is presented by Norris [2]. Herein, we numerically compare isotropic counterparts of a generally anisotropic Hookean solid according to the Frobenius-36 norm and Frobenius-21 norm, to which we refer as F_{36} and F_{21} , respectively, as well as according to the operator norm, to which we refer as λ . Also, for the case of reduction of a transversely isotropic tensor to its isotropic counterpart, we consider the L_2 slowness-curve fit. Subsequently, to examine the importance in different results obtained with different norms, we use perturbation techniques to examine the effect of errors on isotropic counterparts.

This paper is an examination of a reduction of an anisotropic tensor to isotropy. Reducing a generally anisotropic tensor—with different norms—to a higher symmetry has been a research topic in which two of the authors have engaged for a decade. Consequently, to avoid unnecessary repetitions, we provide references to papers that include proofs, explanations and descriptions of methodologies: Bos and Slawinski [3], Bucataru and Slawinski [4], Danek et al. [5, 6], Danek and Slawinski [7, 8], Diner et al. [9], Kochetov and Slawinski [10, 11, 12], Slawinski [13]. Also, these papers include references to many previous publications of other authors upon which our discussions are based, such as the original work of Gazis et al. [14].

The purpose of this paper is the study of similarity and dissimilarity among different-norm counterparts for both general Hookean solids and the ones commonly used in seismological models. The former case is restricted solely to the stability conditions of the tensor; the latter is limited to values encountered in modelling terrestrial materials. An examination of results of reductions under different norms has not been addressed in the any of the above-mentioned papers, except for a brief comment by Bos and Slawinski [3]. Nor, as far as the authors are able to ascertain, has it been addressed anywhere else.

^aDepartment of Geoinformatics and Applied Computer Science, AGH-University of Science and Technology, Kraków, Poland

^bDepartment of Earth Sciences, Memorial University, St. John's, Newfoundland, A1B 3X5, Canada

2 Elasticity tensors

For convenience of referring to standard expressions, let us state the following. A Hookean solid, c_{ijkl} , is a mathematical object defined by Hooke's Law,

$$\sigma_{ij} = \sum_{k=1}^3 \sum_{\ell=1}^3 c_{ijkl} \varepsilon_{k\ell}, \quad i, j = 1, 2, 3, \quad (1)$$

where σ_{ij} , $\varepsilon_{k\ell}$ and c_{ijkl} are the stress, strain and elasticity tensors, respectively. The components of the elasticity tensor can be written—in Kelvin's, as opposed to Voigt's, notation (e.g., Chapman [15])—as a symmetric second-rank tensor in \mathbb{R}^6 ,

$$C = \begin{bmatrix} c_{1111} & c_{1122} & c_{1133} & \sqrt{2}c_{1123} & \sqrt{2}c_{1113} & \sqrt{2}c_{1112} \\ c_{1122} & c_{2222} & c_{2233} & \sqrt{2}c_{2223} & \sqrt{2}c_{2213} & \sqrt{2}c_{2212} \\ c_{1133} & c_{2233} & c_{3333} & \sqrt{2}c_{3323} & \sqrt{2}c_{3313} & \sqrt{2}c_{3312} \\ \sqrt{2}c_{1123} & \sqrt{2}c_{2223} & \sqrt{2}c_{3323} & 2c_{2323} & 2c_{2313} & 2c_{2312} \\ \sqrt{2}c_{1113} & \sqrt{2}c_{2213} & \sqrt{2}c_{3313} & 2c_{2313} & 2c_{1313} & 2c_{1312} \\ \sqrt{2}c_{1112} & \sqrt{2}c_{2212} & \sqrt{2}c_{3312} & 2c_{2312} & 2c_{1312} & 2c_{1212} \end{bmatrix}. \quad (2)$$

If the elasticity tensor is transversely isotropic, its components can be written—in a coordinate system whose x_3 -axis coincides with the rotation-symmetry axis—as

$$C^{\text{TI}} = \begin{bmatrix} c_{1111}^{\text{TI}} & c_{1122}^{\text{TI}} & c_{1133}^{\text{TI}} & 0 & 0 & 0 \\ c_{1122}^{\text{TI}} & c_{1111}^{\text{TI}} & c_{1133}^{\text{TI}} & 0 & 0 & 0 \\ c_{1133}^{\text{TI}} & c_{1133}^{\text{TI}} & c_{3333}^{\text{TI}} & 0 & 0 & 0 \\ 0 & 0 & 0 & 2c_{2323}^{\text{TI}} & 0 & 0 \\ 0 & 0 & 0 & 0 & 2c_{2323}^{\text{TI}} & 0 \\ 0 & 0 & 0 & 0 & 0 & c_{1111}^{\text{TI}} - c_{1122}^{\text{TI}} \end{bmatrix}. \quad (3)$$

If the elasticity tensor is isotropic, its components can be written—in any coordinate system—as

$$C^{\text{iso}} = \begin{bmatrix} c_{1111}^{\text{iso}} & c_{1111}^{\text{iso}} - 2c_{2323}^{\text{iso}} & c_{1111}^{\text{iso}} - 2c_{2323}^{\text{iso}} & c_{1111}^{\text{iso}} - 2c_{2323}^{\text{iso}} & 0 & 0 & 0 \\ c_{1111}^{\text{iso}} - 2c_{2323}^{\text{iso}} & c_{1111}^{\text{iso}} & c_{1111}^{\text{iso}} - 2c_{2323}^{\text{iso}} & c_{1111}^{\text{iso}} - 2c_{2323}^{\text{iso}} & 0 & 0 & 0 \\ c_{1111}^{\text{iso}} - 2c_{2323}^{\text{iso}} & c_{1111}^{\text{iso}} - 2c_{2323}^{\text{iso}} & c_{1111}^{\text{iso}} - 2c_{2323}^{\text{iso}} & c_{1111}^{\text{iso}} - 2c_{2323}^{\text{iso}} & 0 & 0 & 0 \\ 0 & 0 & 0 & 0 & 2c_{2323}^{\text{iso}} & 0 & 0 \\ 0 & 0 & 0 & 0 & 0 & 2c_{2323}^{\text{iso}} & 0 \\ 0 & 0 & 0 & 0 & 0 & 0 & 2c_{2323}^{\text{iso}} \end{bmatrix}, \quad (4)$$

and expression (1) can be rewritten as

$$\sigma_{ij} = c_{1111}^{\text{iso}} \delta_{ij} \sum_{k=1}^3 \varepsilon_{kk} + 2c_{2323}^{\text{iso}} \varepsilon_{ij}, \quad i, j = 1, 2, 3.$$

3 Norms

To examine the closeness between elasticity tensors, as discussed by Bos and Slawinski [3] and by DaneK et al. [5, 6], we consider several norms.

3.1 Frobenius norms

The Frobenius norm treats a matrix in $\mathbb{R}^{n \times n}$ as a Euclidean vector in \mathbb{R}^{n^2} . In the case of a symmetric 6×6 matrix, where $C_{mn} = C_{nm}$, we can choose either

$$\|C\|_{F_{36}} = \sqrt{\sum_{m=1}^6 \sum_{n=1}^6 C_{mn}^2},$$

which uses the thirty-six components, including their coefficients of $\sqrt{2}$ and 2, or

$$\|C\|_{F_{21}} = \sqrt{\sum_{m=1}^6 \sum_{n=1}^m C_{mn}^2},$$

which uses only the twenty-one independent components, including their coefficients of $\sqrt{2}$ and 2.

3.2 Operator norm

As discussed by Bos and Slawinski [3], by treating a matrix as a vector, the Frobenius norms ignore the fact that a matrix is a representation of a linear map from \mathbb{R}^n to \mathbb{R}^n . In view of equation (1), the elasticity tensor represents a linear map between the strain tensor, whose components can be expressed as a symmetric 3×3 matrix, $[\varepsilon_{kl}]$, and the stress tensor, whose components can be expressed as a symmetric 3×3 matrix, $[\sigma_{ij}]$. The operator norm of the elasticity tensor considered as a mapping from $\mathbb{R}^{3 \times 3}$ to $\mathbb{R}^{3 \times 3}$, where both the stress and strain tensors are endowed with the Frobenius norm, F_9 , is the operator norm of matrix $C \in \mathbb{R}^{6 \times 6}$.

Given a norm on \mathbb{R}^n , the associated operator norm of matrix $A \in \mathbb{R}^{n \times n}$ is

$$\|A\| := \max_{\|x\|=1} \|Ax\|.$$

An example of such a norm is the Euclidean operator norm, which—for symmetric matrices—becomes

$$\|A\|_2 := \max\{|\lambda| : \lambda \text{ an eigenvalue of } A\}.$$

The operator norm of an elasticity tensor—whose components in a given coordinate system can be expressed as a symmetric 6×6 matrix—is

$$\|C\|_\lambda = \max |\lambda_i|,$$

where $\lambda_i \in \{\lambda_1, \dots, \lambda_6\}$ is an eigenvalue of C .

4 Slowness-curve L_2 fit

In a manner similar to the F_{36} norm, F_{21} norm and operator norm, the slowness-curve L_2 fit can be used to find an isotropic counterpart to an anisotropic Hookean solid. However, in contrast to these norms, which rely on finding the smallest distance between tensors, it relies on finding the best fit of circles—according to a chosen criterion—to noncircular wavefronts.

To consider a generally anisotropic tensor, one would need to fit a sphere into a slowness surface. However, for the purpose of insightful graphical illustrations, we consider a transversely isotropic tensor obtained from a generally anisotropic one, since its directional dependence reduces to two dimensions.

For both the operator norm and fitting, would it be spheres or circles, we do not invoke explicit expressions for the components of the closest elasticity tensor, as we do for the Frobenius norms, but instead we examine the effect of these components on certain quantities. For the operator norm, this quantity consists of eigenvalues; for the fit, this quantity consists of wavefront slownesses.

The direct results of the norms are the components of the corresponding isotropic tensors, and the wavefront-slowness circles are their consequences. The direct result of the slowness-curve fit are slowness circles, and the components of the corresponding isotropic tensor are their consequence.

Herein, the best fit, in the L_2 sense, is the radius, r , that minimizes

$$S = \sum_{i=1}^n (s_i - r_i)^2, \quad (5)$$

where s_i are n discretized values along the slowness curve, and $s_i - r_i$ is measured in the radial direction. Hence, r is the radius of the slowness circle; it corresponds to isotropy.

5 Numerical results

5.1 Isotropic counterparts of general Hookean solids

In this section, we investigate isotropic counterparts derived using the three norms introduced in Section 3. We do so for the most general Hookean solids. In other words, their material symmetry is a general anisotropy, and their parameter values are allowed to vary randomly over a large range. The sole restriction on these values is the stability condition of the solid. This condition is tantamount to the positive definiteness of matrix (2), which is equivalent to its eigenvalues being positive.

Consider Figures 1 and 2. Both figures result from ten thousand repetitions of the tensor whose general form is stated in expression (2). All histograms in this paper are generated by ten thousand repetitions, which are expressed by the total height of all blocks; the interpretation of each histogram relies on the relative heights of these blocks. Herein, the values of the density-scaled elasticity parameters, whose units are km^2/s^2 , are allowed to vary randomly between 0 and 20, on the main diagonal of matrix (2), and between -10 and 10 , otherwise. The positive range, $(0, 20)$, along the main diagonal, is required by the positive definiteness of the elasticity tensor.

The histograms in Figures 1 illustrate the values of the elasticity parameters of an isotropic counterpart—according to the F_{21} norm—and normalized by the values of the corresponding parameter according to the F_{36} norm. If both norms result in the same value of the parameter, their ratio is equal to unity. The histograms in Figures 2 illustrate the values of the elasticity parameters of an isotropic counterpart—according to the operator norm—and also normalized by the values of the corresponding parameter according to the F_{36} norm.

Examining Figures 1 and 2, we see that highest values of the histograms appear in the neighbourhood of unity. Thus, we infer that the three norms result in similar isotropic counterparts of a general Hookean solid. Recognizing that the scale of the horizontal axes is different for each plot, we see that the histograms of the operator norm are broader than for the F_{21} norm. It means that the F_{36} norm is more similar to the F_{21} norm than to the operator norm.

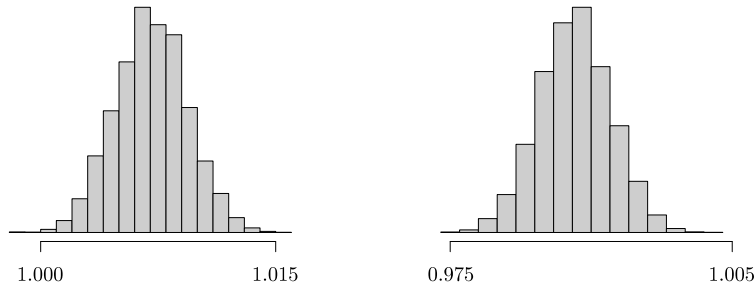


Figure 1: Deviation of c_{1111}^{iso} and c_{2323}^{iso} for general Hookean solid, according to F_{21} , and normalized by corresponding F_{36} parameters

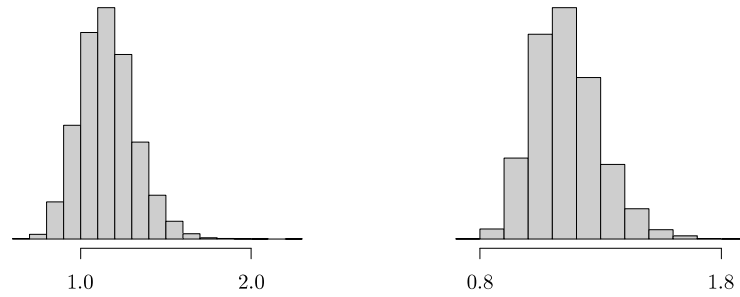


Figure 2: Deviation of c_{1111}^{iso} and c_{2323}^{iso} for general Hookean solid, according to operator norm, and normalized by corresponding F_{36} parameters

To enquire into that behaviour, we examine Figure 3. On the horizontal axis is the ratio of the largest eigenvalue to the sum of the remaining eigenvalues. The quantities of the vertical axis are the same as for the horizontal axis in Figure 2. As expected from its definition, the operator norm, which is the value of the largest eigenvalue, is sensitive to that ratio. Quantitatively, the correlation between the ratio and the breadth of the histogram for c_{1111}^{iso} has the coefficient of 0.7210, and for c_{2323}^{iso} of 0.8578; there is a significant correlation.

The similarity of the results obtained according to the F_{21} and F_{36} norms is a consequence of the fact that they differ by the weight on the offdiagonal terms. These terms, however, tend to be smaller than the main-diagonal terms due to the requirement of positive definiteness.

5.2 Isotropic counterparts of seismological Hookean solids

Let us consider a case of a Hookean solid that is pertinent to common terrestrial materials near the Earth’s surface. For that purpose, we use the elasticity tensor obtained by Dewangan and Grechka [16] from measurements of vertical seismic profiling,

$$C = \begin{bmatrix} 7.8195 & 3.4495 & 2.5667 & \sqrt{2}(0.1374) & \sqrt{2}(0.0558) & \sqrt{2}(0.1239) \\ 3.4495 & 8.1284 & 2.3589 & \sqrt{2}(0.0812) & \sqrt{2}(0.0735) & \sqrt{2}(0.1692) \\ 2.5667 & 2.3589 & 7.0908 & \sqrt{2}(-0.0092) & \sqrt{2}(0.0286) & \sqrt{2}(0.1655) \\ \sqrt{2}(0.1374) & \sqrt{2}(0.0812) & \sqrt{2}(-0.0092) & 2(1.6636) & 2(-0.0787) & 2(0.1053) \\ \sqrt{2}(0.0558) & \sqrt{2}(0.0735) & \sqrt{2}(0.0286) & 2(-0.0787) & 2(2.0660) & 2(-0.1517) \\ \sqrt{2}(0.1239) & \sqrt{2}(0.1692) & \sqrt{2}(0.1655) & 2(0.1053) & 2(-0.1517) & 2(2.4270) \end{bmatrix}. \quad (6)$$

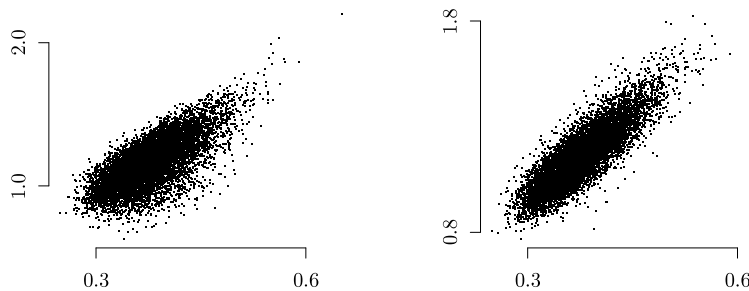


Figure 3: Relation between deviations illustrated in Figure 2 and corresponding spreads of eigenvalues

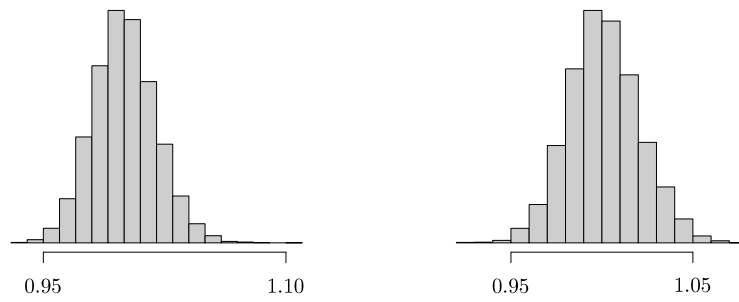


Figure 4: Deviation of c_{1111}^{iso} and c_{2323}^{iso} for tensor (6), according to F_{21} , and normalized by corresponding F_{36} parameters

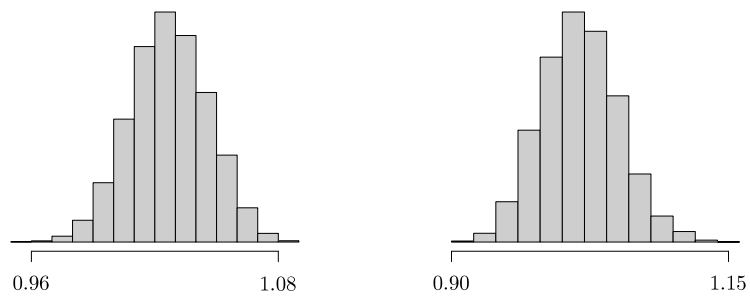


Figure 5: Deviation of c_{1111}^{iso} and c_{2323}^{iso} for tensor (6), according to operator norm, and normalized by corresponding F_{36} parameters

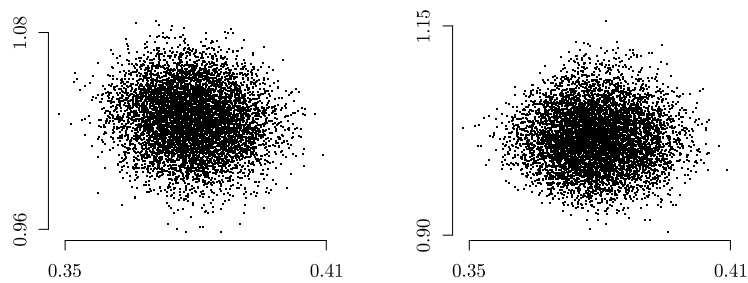


Figure 6: Relation between deviation illustrated in Figure 5 and corresponding spreads of eigenvalues

Its components are density-scaled elasticity parameters; their units are km^2/s^2 . Herein, the parameter values are more restricted than for a general Hookean solid examined in Section 5.1.

Consider Figures 4 and 5, which are generated using tensor (6), and its errors (Grechka, pers. comm., 2007),

$$\pm \begin{bmatrix} 0.1656 & 0.1122 & 0.1216 & 0.1176 & 0.0774 & 0.0741 \\ 0.1122 & 0.1862 & 0.1551 & 0.0797 & 0.1137 & 0.0832 \\ 0.1216 & 0.1551 & 0.1439 & 0.0856 & 0.0662 & 0.1010 \\ 0.1176 & 0.0797 & 0.0856 & 0.0714 & 0.0496 & 0.0542 \\ 0.0774 & 0.1137 & 0.0662 & 0.0496 & 0.0626 & 0.0621 \\ 0.0741 & 0.0832 & 0.1010 & 0.0542 & 0.0621 & 0.0802 \end{bmatrix}, \quad (7)$$

which are the estimates of the standard deviations corresponding to each component of expression (6), in the coordinate system of data acquisition, since these values do not constitute components of a tensor. Either figure results from ten thousand repetitions. The values of the elasticity parameters are allowed to vary randomly with a uniform distribution up to three standard deviations stated in matrix (7). Figures 4 and 5 are analogous to Figures 1 and 2, respectively, except that—by considering tensor (6) and its standard deviations—the general Hookean solid is restricted to values that are representative for seismological models of the Earth's crust.

Comparing Figures 1 and 4, and recognizing that the scale of the horizontal axes is different for each plot, we see that the Frobenius norms produce isotropic counterparts for tensor (6) that are as close to one another as for the isotropic counterparts of a general Hookean solid. This conclusion is confirmed quantitatively.

For the left plot of Figure 1, the mean value is 1.0071, and for the left plot of Figure 4, the mean value is 1.0002. For the right plot of Figure 1, the mean value is 1.0011, and for the right plot of Figure 4 the mean value is 0.9882. Thus, the values for a seismological Hookean solid remain similarly close to unity as they do for a general Hookean solid, which is symptomatic of both Frobenius norms resulting in similar isotropic counterparts for a wide range of generally anisotropic tensors.

Comparing Figures 2 and 5, and recognizing that scales of the horizontal axes are different, we see that the operator norm produces isotropic counterparts for tensor (6) whose scatter is narrower than for a general Hookean solid. Quantitatively, for the left plot of Figure 2, the standard deviation is 0.1624, and for the left plot of Figure 5, it is 0.019; for the right plots of these figures, the corresponding standard deviations are 0.1373 and 0.0348, respectively.

To explain that behaviour we see that, in contrast to a general Hookean solid and Figure 3, the correlation between the ratio of the eigenvalues and the breadth of the histograms does not appear, as illustrated in Figure 6, where the quantities of the vertical axis are the same as for the horizontal axis in Figure 5. We can infer that—in the case of a seismological Hookean solid grounded in empirical information—the eigenvalues of the elasticity tensor are more similar to each other than in the case of a general Hookean solid, whose elasticity parameters can assume any value as long as the tensor remains positive-definite.

5.3 Tensor C_a^{TI}

To graphically illustrate the results for different norms and to examine further their properties, let us—without any significant loss of generality—consider a transversely isotropic tensor. We choose a tensor computed by Danek et al. [6], which is the closest counterpart, in the F_{36} sense, of tensor (6),

$$C_a^{\text{TI}} = \begin{bmatrix} 8.0641 & 3.3720 & 2.4588 & 0 & 0 & 0 \\ 3.3720 & 8.0641 & 2.4588 & 0 & 0 & 0 \\ 2.4588 & 2.4588 & 7.0817 & 0 & 0 & 0 \\ 0 & 0 & 0 & 2(1.8625) & 0 & 0 \\ 0 & 0 & 0 & 0 & 2(1.8625) & 0 \\ 0 & 0 & 0 & 0 & 0 & 2(2.3460) \end{bmatrix}. \quad (8)$$

The slowness curves for tensor (8) and its isotropic counterpart circles discussed in Sections 5.3.1, 5.3.2 and 5.3.3, below, are shown in Figure 7. Isotropic tensors examined in this section are counterparts of this tensor.

For the purpose of this section, the choice of norm to obtain tensor (8) from its generally anisotropic origins is insignificant, provided the result is transversely isotropic. One could even begin with a generic transversely isotropic tensor, without relating it to a generally anisotropic one. We derive the transversely isotropic tensor from a generally anisotropic one inferred from seismic measurement in order to examine values commonly encountered in geophysics. Also, one could use this generally anisotropic tensor itself and find its isotropic counterparts, as in Section 5.2. However, we choose to consider the isotropic counterparts of a transversely isotropic tensor to be able to illustrate them graphically, as shown in Figures 7–11, below. To enhance the details, in each case, only the first quadrant is shown, since—due to symmetry—no further information is provided by the remaining quadrants.

5.3.1 F_{36} norm

Let us consider the Frobenius norm for the thirty-six components. There are analytical formulæ to calculate—from a generally anisotropic tensor—the two parameters of its closest isotropic tensor (Voigt, [17]). From a transversely isotropic tensor, these parameters are

$$c_{1111}^{\text{iso}F_{36}} = \frac{1}{15} (8c_{1111}^{\text{TI}} + 4c_{1133}^{\text{TI}} + 8c_{2323}^{\text{TI}} + 3c_{3333}^{\text{TI}})$$

and

$$c_{2323}^{\text{iso}F_{36}} = \frac{1}{30} (7c_{1111}^{\text{TI}} - 5c_{1122}^{\text{TI}} - 4c_{1133}^{\text{TI}} + 12c_{2323}^{\text{TI}} + 2c_{3333}^{\text{TI}}).$$

Hence, the closest isotropic counterpart of tensor (8) is

$$C_a^{\text{iso}_{F_{36}}} = \begin{bmatrix} 7.3662 & 2.9484 & 2.9484 & 0 & 0 & 0 \\ 2.9484 & 7.3662 & 2.9484 & 0 & 0 & 0 \\ 2.9484 & 2.9484 & 7.3662 & 0 & 0 & 0 \\ 0 & 0 & 0 & 2(2.2089) & 0 & 0 \\ 0 & 0 & 0 & 0 & 2(2.2089) & 0 \\ 0 & 0 & 0 & 0 & 0 & 2(2.2089) \end{bmatrix}. \quad (9)$$

5.3.2 F_{21} norm

Let us consider the Frobenius norm for the twenty-one independent components. Following Slawinski [13], for a transversely isotropic tensor, the analytical formulae to calculate the two parameters of its closest isotropic tensor are

$$c_{1111}^{\text{iso}_{F_{21}}} = \frac{1}{9} (5c_{1111}^{\text{TI}} + 2c_{1133}^{\text{TI}} + 4c_{2323}^{\text{TI}} + 2c_{3333}^{\text{TI}})$$

and

$$c_{2323}^{\text{iso}_{F_{21}}} = \frac{1}{18} (4c_{1111}^{\text{TI}} - 3c_{1122}^{\text{TI}} - 2c_{1133}^{\text{TI}} + 8c_{2323}^{\text{TI}} + c_{3333}^{\text{TI}}).$$

Hence,

$$C_a^{\text{iso}_{F_{21}}} = \begin{bmatrix} 7.4279 & 3.0716 & 3.0716 & 0 & 0 & 0 \\ 3.0716 & 7.4279 & 3.0716 & 0 & 0 & 0 \\ 3.0716 & 3.0716 & 7.4279 & 0 & 0 & 0 \\ 0 & 0 & 0 & 2(2.1781) & 0 & 0 \\ 0 & 0 & 0 & 0 & 2(2.1781) & 0 \\ 0 & 0 & 0 & 0 & 0 & 2(2.1781) \end{bmatrix}. \quad (10)$$

5.3.3 λ norm

Unlike the Frobenius norms, the operator norm has no analytical formulae for $c_{1111}^{\text{iso}_\lambda}$ and $c_{2323}^{\text{iso}_\lambda}$. They must be obtained numerically. The largest eigenvalues are obtained using a standard numerical procedure of the Singular Value Decomposition and then optimized over a two-dimensional solution space using a similar procedure to the one described in Danek et al. [6]. For tensor (8), we obtain

$$C_a^{\text{iso}_\lambda} = \begin{bmatrix} 7.7562 & 3.0053 & 3.0053 & 0 & 0 & 0 \\ 3.0053 & 7.7562 & 3.0053 & 0 & 0 & 0 \\ 3.0053 & 3.0053 & 7.7562 & 0 & 0 & 0 \\ 0 & 0 & 0 & 2(2.3755) & 0 & 0 \\ 0 & 0 & 0 & 0 & 2(2.3755) & 0 \\ 0 & 0 & 0 & 0 & 0 & 2(2.3755) \end{bmatrix}. \quad (11)$$

5.3.4 Distances among tensors

To gain insight into different isotropic counterparts of tensor (8), we calculate the F_{36} distance between tensors (9) and (11), which is 0.8993. The F_{36} distance between tensors (8) and (9) is 1.8461. The F_{36} distance between tensors (8) and (11) is 2.0535, where we note that tensor (11) is the closest isotropic tensor according to the operator—not the F_{36} —norm. Thus, in spite of similarities between the isotropic tensors, the distance between them is large in comparison to their distances to tensor (8).

This is an illustration of abstractness of the concept of distances in the space of elasticity tensors. A concrete evaluation is provided by comparing the results obtained by minimizing these distances. Such results are tensors (9), (10), (11), and their wavefront-slowness circles in Figure 7. This figure illustrates a similarity among these circles, which is a realm in which the isotropic tensors can be compared. They can be compared within the slowness space.

5.4 Comparison of norms

Comparing tensors (9), (10) and (11), we see that the parameters of the closest isotropic tensor depend on the norm used. Given two anisotropic tensors, we might be interested to know which of them is closer to isotropy. For a given norm, an answer is obtained by a straightforward calculation. In general, for different norms, there is no absolute answer: the sequence in closeness to isotropy can be reversed between two tensors; it depends on the norms.

5.4.1 F_{36} versus F_{21}

Using a numerical search based on a simple random walk through a solution space with the target function being a difference between the minimized F_{21} distance and the maximized F_{36} distance, an elasticity tensor is generated that is further from isotropy than tensor (8) according to the F_{36} norm, but closer to isotropy than tensor (8) according to the F_{21} norm. The search results in

$$C_b^{\text{TI}} = \begin{bmatrix} 7.3091 & 4.5882 & 2.9970 & 0 & 0 & 0 \\ 4.5882 & 7.3091 & 2.9970 & 0 & 0 & 0 \\ 2.9970 & 2.9970 & 6.6604 & 0 & 0 & 0 \\ 0 & 0 & 0 & 2(1.5631) & 0 & 0 \\ 0 & 0 & 0 & 0 & 2(1.5631) & 0 \\ 0 & 0 & 0 & 0 & 0 & 2(1.3605) \end{bmatrix}, \quad (12)$$

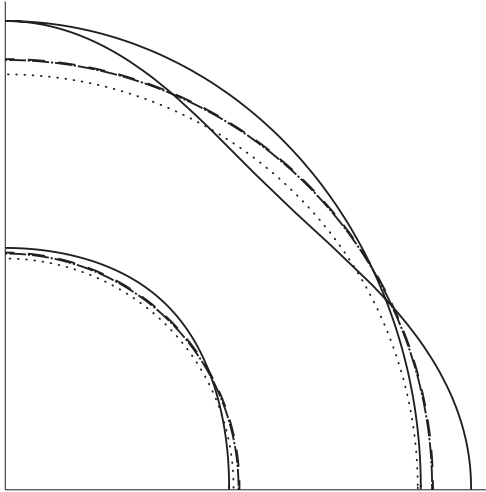


Figure 7: Slowness curves for tensor (8): solid lines represent the qP , qSV and SH waves; dashed lines represent the P and S waves according to F_{36} norm; dashed-dotted lines represent the P and S waves according to F_{21} norm; the results of these norms almost coincide; dotted lines represent the P and S waves according to λ norm.

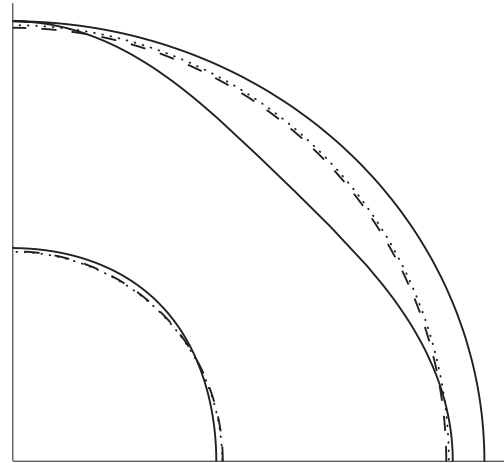


Figure 8: Slowness curves for tensor (12): solid lines represent the qP , qSV and SH waves; dashed lines represent the P and S waves according to F_{36} norm; dotted lines represent the P and S waves according to F_{21} norm.

with its corresponding isotropic counterparts,

$$C_b^{iso_{F_{36}}} = \begin{bmatrix} 6.8631 & 3.6422 & 3.6422 & 0 & 0 & 0 \\ 3.6422 & 6.8631 & 3.6422 & 0 & 0 & 0 \\ 3.6422 & 3.6422 & 6.8631 & 0 & 0 & 0 \\ 0 & 0 & 0 & 2(1.6104) & 0 & 0 \\ 0 & 0 & 0 & 0 & 2(1.6104) & 0 \\ 0 & 0 & 0 & 0 & 0 & 2(1.6104) \end{bmatrix} \quad (13)$$

and

$$C_b^{iso_{F_{21}}} = \begin{bmatrix} 6.9014 & 3.7188 & 3.7188 & 0 & 0 & 0 \\ 3.7188 & 6.9014 & 3.7188 & 0 & 0 & 0 \\ 3.7188 & 3.7188 & 6.9014 & 0 & 0 & 0 \\ 0 & 0 & 0 & 2(1.5913) & 0 & 0 \\ 0 & 0 & 0 & 0 & 2(1.5913) & 0 \\ 0 & 0 & 0 & 0 & 0 & 2(1.5913) \end{bmatrix}, \quad (14)$$

respectively. The distances to isotropy for C_a^{TI} and C_b^{TI} —stated, respectively, in expressions (8) and (12)—using the F_{36} and F_{21} norms, are

$$\begin{aligned} d_{a_{36}} &= 1.8460 < d_{b_{36}} = 2.0400, \\ d_{a_{21}} &= 1.6372 > d_{b_{21}} = 1.5517. \end{aligned}$$

The slowness curves for tensor (12) and its isotropic counterparts are shown in Figure 8.

5.4.2 F_{36} versus λ

The second comparison is between the F_{36} norm and the λ norm. We obtain

$$C_{bb}^{\text{TI}} = \begin{bmatrix} 6.8639 & 3.3046 & 2.8770 & 0 & 0 & 0 \\ 3.3046 & 6.8639 & 2.8770 & 0 & 0 & 0 \\ 2.8770 & 2.8770 & 8.3825 & 0 & 0 & 0 \\ 0 & 0 & 0 & 2(2.7744) & 0 & 0 \\ 0 & 0 & 0 & 0 & 2(2.7744) & 0 \\ 0 & 0 & 0 & 0 & 0 & 2(1.7797) \end{bmatrix}, \quad (15)$$

which is further from isotropy according to the F_{36} norm and closer to isotropy according to the λ norm. Its isotropic counterparts in the sense of the F_{36} and λ norms are

$$C_{bb}^{iso_{F_{36}}} = \begin{bmatrix} 7.5842 & 2.9125 & 2.9125 & 0 & 0 & 0 \\ 2.9125 & 7.5842 & 2.9125 & 0 & 0 & 0 \\ 2.9125 & 2.9125 & 7.5842 & 0 & 0 & 0 \\ 0 & 0 & 0 & 2(2.3358) & 0 & 0 \\ 0 & 0 & 0 & 0 & 2(2.3358) & 0 \\ 0 & 0 & 0 & 0 & 0 & 2(2.3358) \end{bmatrix} \quad (16)$$

and

$$C_{bbb}^{\text{iso}\lambda} = \begin{bmatrix} 7.4712 & 2.9171 & 2.9171 & 0 & 0 & 0 \\ 2.9171 & 7.4712 & 2.9171 & 0 & 0 & 0 \\ 2.9171 & 2.9171 & 7.4712 & 0 & 0 & 0 \\ 0 & 0 & 0 & 2(2.7704) & 0 & 0 \\ 0 & 0 & 0 & 0 & 2(2.7704) & 0 \\ 0 & 0 & 0 & 0 & 0 & 2(2.7704) \end{bmatrix}, \quad (17)$$

respectively. The distances to isotropy for C_a^{TI} and C_{bb}^{TI} , using the F_{36} and λ norms, are

$$d_{a_{36}} = 1.8460 < d_{bb_{36}} = 2.1825, \\ d_{a_\lambda} = 1.0259 > d_{bb_\lambda} = 0.9947.$$

The slowness curves for tensor (15) and its isotropic counterparts are shown in Figure 9.

5.4.3 F_{21} versus λ

The third comparison is between the F_{21} norm and the λ norm. The resulting tensor is

$$C_{bbb}^{\text{TI}} = \begin{bmatrix} 4.5706 & 2.6852 & 2.9075 & 0 & 0 & 0 \\ 2.6852 & 4.5706 & 2.9075 & 0 & 0 & 0 \\ 2.9075 & 2.9075 & 5.2705 & 0 & 0 & 0 \\ 0 & 0 & 0 & 2(1.9145) & 0 & 0 \\ 0 & 0 & 0 & 0 & 2(1.9145) & 0 \\ 0 & 0 & 0 & 0 & 0 & 2(0.9427) \end{bmatrix}, \quad (18)$$

with isotropic counterparts according to the F_{21} norm and the λ norm,

$$C_{bbb}^{\text{iso}F_{21}} = \begin{bmatrix} 5.2074 & 2.4297 & 2.4297 & 0 & 0 & 0 \\ 2.4297 & 5.2074 & 2.4297 & 0 & 0 & 0 \\ 2.4297 & 2.4297 & 5.2074 & 0 & 0 & 0 \\ 0 & 0 & 0 & 2(1.3889) & 0 & 0 \\ 0 & 0 & 0 & 0 & 2(1.3889) & 0 \\ 0 & 0 & 0 & 0 & 0 & 2(1.3889) \end{bmatrix} \quad (19)$$

and

$$C_{bbb}^{\text{iso}\lambda} = \begin{bmatrix} 5.2926 & 2.4354 & 2.4354 & 0 & 0 & 0 \\ 2.4354 & 5.2926 & 2.4354 & 0 & 0 & 0 \\ 2.4354 & 2.4354 & 5.2926 & 0 & 0 & 0 \\ 0 & 0 & 0 & 2(1.4286) & 0 & 0 \\ 0 & 0 & 0 & 0 & 2(1.4286) & 0 \\ 0 & 0 & 0 & 0 & 0 & 2(1.4286) \end{bmatrix}, \quad (20)$$

respectively. The distances to isotropy for both C_a^{TI} and C_{bbb}^{TI} using the F_{21} and λ norms are

$$d_{a_{21}} = 1.6372 < d_{bbb_{21}} = 2.0842, \\ d_{a_\lambda} = 1.0259 > d_{bbb_\lambda} = 0.9719.$$

The slowness curves for tensor (18) and its isotropic counterparts are shown in Figure 10.

5.5 Slowness-curve fit

Considering tensor (8) and applying a minimization for the qP wave, using formula (5), we find $S = 0.0886$ with $r = 0.3770$. Following the same procedure for the qSV and SH waves, we find $S = 0.2973$, with $r = 0.6832$, and $S = 0.2169$, with $r = 0.6831$, respectively. Combining these results, we obtain $S = 0.6029$, with $r_p = 0.3770$ and $r_s = 0.6831$, which are the slownesses of the P and S waves, respectively. Note that—since the slowness curves of the qP waves are detached from the curves for the qSV and SH waves—the value of r for the P waves does not change by combining the results.

Since $v_p = \sqrt{c_{1111}}$ and $v_s = \sqrt{c_{2323}}$ are the P -wave and S -wave speeds, respectively, it follows that $c_{1111} = 1/r_p^2$ and $c_{2323} = 1/r_s^2$. Hence, we obtain

$$C_a^{\text{iso}L_2} = \begin{bmatrix} 7.0341 & 2.7485 & 2.7485 & 0 & 0 & 0 \\ 2.7485 & 7.0341 & 2.7485 & 0 & 0 & 0 \\ 2.7485 & 2.7485 & 7.0341 & 0 & 0 & 0 \\ 0 & 0 & 0 & 2(2.1428) & 0 & 0 \\ 0 & 0 & 0 & 0 & 2(2.1428) & 0 \\ 0 & 0 & 0 & 0 & 0 & 2(2.1428) \end{bmatrix}. \quad (21)$$

The slowness curves for tensor (21) and its isotropic counterparts are shown in Figure 11.

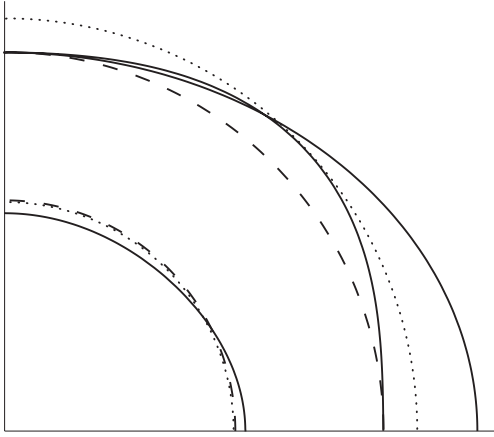


Figure 9: Slowness curves for tensor (15): solid lines represent the qP , qSV and SH waves; dotted lines represent its P and S waves according to F_{36} norm; dashed lines represent its P and S waves according to λ norm.

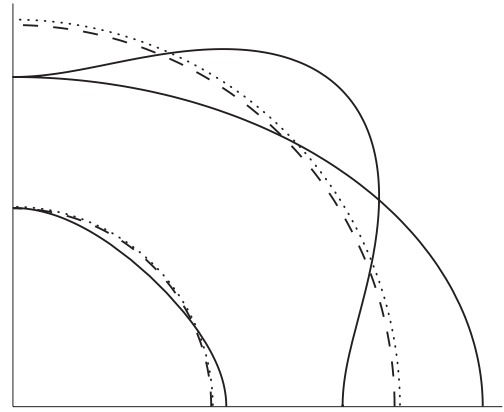


Figure 10: Slowness curves for tensor (18): solid lines represent the qP , qSV and SH waves; dotted lines represent its P and S waves according to F_{21} norm; dashed lines represent its P and S waves according to λ norm.

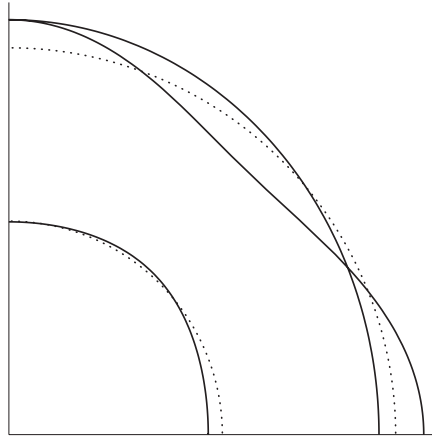


Figure 11: Slowness curves for tensor (21): solid lines represent the qP , qSV and SH waves; dotted lines represent its P and S waves according to the slowness-curve L_2 fit.

5.6 Thomsen parameters

To consider the empirical importance of the numerical study presented in Section 5, we examine whether or not tensors (8), (12), (15) and (18) might be representative of seismic media. Herein, we show that these tensors exhibit the strength of anisotropy that is consistent with cases of interest to geophysicists. To show this consistency, we calculate the Thomsen [18] parameters,

$$\begin{aligned}\alpha &= \sqrt{c_{3333}^{\text{TI}}}, \\ \beta &= \sqrt{c_{2323}^{\text{TI}}}, \\ \gamma &= \frac{c_{1212}^{\text{TI}} - c_{2323}^{\text{TI}}}{2c_{2323}^{\text{TI}}}, \\ \delta &= \frac{(c_{1133}^{\text{TI}} + c_{2323}^{\text{TI}})^2 - (c_{3333}^{\text{TI}} - c_{2323}^{\text{TI}})^2}{2c_{3333}^{\text{TI}}(c_{3333}^{\text{TI}} - c_{2323}^{\text{TI}})}, \\ \epsilon &= \frac{c_{1111}^{\text{TI}} - c_{3333}^{\text{TI}}}{2c_{3333}^{\text{TI}}}.\end{aligned}$$

The values of these parameters for tensors (8), (12), (15) and (18) are shown in Table 1. Comparing results of this table to data of Auld [19] and Thomsen [18], we see that these tensors represent common geological materials.

Tensor	α	β	γ	δ	ϵ
C_a^{TI}	2.6612	1.2986	0.1956	-0.1561	0.0694
C_b^{TI}	2.5808	1.2503	-0.6483	-0.0764	0.0487
C_{bb}^{TI}	2.2958	1.3837	-0.2538	0.3389	-0.6640
C_{bbb}^{TI}	2.8953	1.6657	-0.1793	0.0052	-0.0906

Table 1: Thomsen parameters for tensors (8), (12), (15) and (18)

5.7 Isotropic counterparts as functions of anisotropy strength

Let us examine the effect of the three norms and the slowness-curve fit as a function of the strength of anisotropy. We take Thomsen’s parameter ϵ to quantify this strength.

For this examination, we choose tensor (9), and vary the value of c_{1111} to obtain the values of ϵ between -0.4 and 1 . This range covers both weak and strong anisotropy. The P -wave slowness values of the isotropic counterparts of the norms and the fit are shown in Figure 12.

As expected, for isotropy, $\epsilon = 0$, the P -wave-slowness values coincide for the three norms and the slowness-curve fit. The common value is $1/\sqrt{c_{1111}^{\text{TI}}} = 1/\sqrt{c_{3333}^{\text{TI}}} = 0.3684$. Also, both Frobenius-norm values, F_{21} and F_{36} , and the operator-norm values, λ , are similar to each other for the entire range of ϵ . Their differences are negligible in the context of measurement errors. However, the values for the slowness-curve fit are similar to the values for the norms only in the vicinity of $\epsilon = 0$. For the fit, the behaviour of the P -wave slowness as a function of ϵ is different, as illustrated by the shape of the graphs.

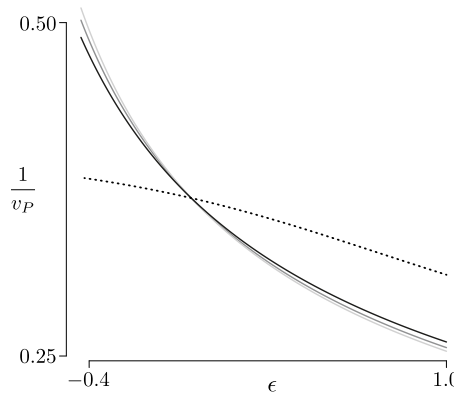


Figure 12: P -wave slowness of isotropic counterparts as function of ϵ of transversely isotropic tensor; F_{21} (light gray), F_{36} (dark gray), λ (black); and L_2 (dotted)

5.8 Error propagation

Components of an anisotropic tensor obtained from experimental measurements exhibit uncertainties due to measurement errors. These uncertainties propagate to its symmetric counterparts.

In-depth studies of probability laws for the stiffness components was a subject of a paper by Guillemot and Soize [20]. In general, the offdiagonal terms may be assumed to be Gaussian but the diagonal ones are Gamma-distribution random variables. The statistical dependence structure for the six strongest symmetry classes, namely, isotropic, TI, cubic, tetragonal, trigonal and orthotropic, is presented in Table 1 of Guillemot and Soize [20]. From the point of view of seismic observations, this problem was analyzed by Rusmanugroho and McMechan [21]. In this case, normality—expressed as a large-shape parameter of the Gamma-distribution variables—and the independence assumptions are good analogies for observations, even though certain components, such as c_{1212} and c_{1223} , have the values of the crosscorrelation matrix significantly higher than others due to the relation between their horizontal and vertical stress and horizontally polarized strain. These assumptions, namely, independence of components and normality of their distributions, are crucial in the approach of Danek et al. [5]. They are also—at least partially—required to obtain matrix (7) through numerical simulations performed by Dewangan and Grechka [16].

Let us examine the error propagation between the transversely isotropic tensor and its isotropic counterparts. Apart from inferring the stability of these counterparts, such an examination allows us to gain an insight into a range of tensors whose values are pertinent to seismological studies. Even though our conclusions stem from a single transversely isotropic tensor, the perturbation of its components is akin to considering a multitude of such tensors.

The standard deviations of components of tensor (6) are given in expression (7). Since these values do not constitute components of a tensor—and, hence, are valid only in the coordinate system of measurements—there is a need for a simulation to

consider error propagation from tensor (6) to tensor (8). Probability distributions of the values of the components of tensor (8)—obtained by a Monte-Carlo simulation (Danek et al. 2013)—are shown in Figures 13, 14, 15, 16, 17. Therein, different histograms have different horizontal scales.

The probability distributions of the two parameters for its isotropic F_{36} counterpart are obtained in the same manner; they are shown in Figure 18. Their mean values are given in tensor (9). In the same figure, we show the probability distributions of parameters for the F_{21} and λ counterparts, whose mean values are given in tensors (10) and (11).

Examining Figure 18, we infer that, for tensors commonly encountered in seismology, their isotropic counterparts obtained with distinct norms might be similar to each other within a typical range of measurement errors. For both Frobenius norms, probability distributions of the corresponding parameters are very similar to one another.

Independently of the parameter values, in Figure 18, we observe their distributions. The distributions for the operator norm are different than for the Frobenius norms. Also, within the operator norm, there is a significant difference between the c_{1111} and c_{2323} distributions. This is a consequence of properties of the operator norm, where only the largest among the six eigenvalues is taken into consideration.

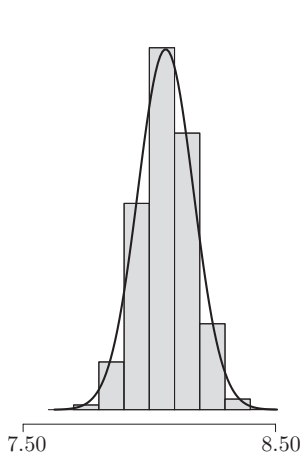


Figure 13: c_{1111} of tensor (8)

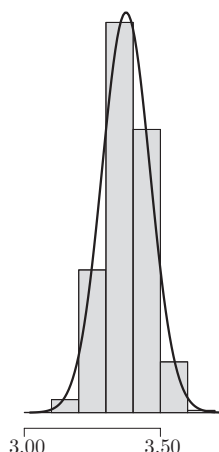


Figure 14: c_{1122} of tensor (8)

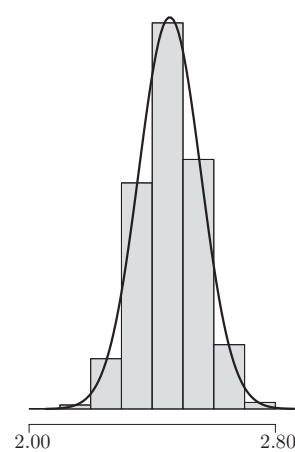


Figure 15: c_{1133} of tensor (8)

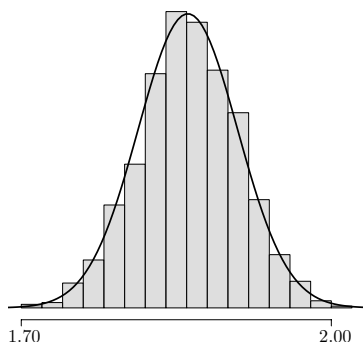


Figure 16: c_{2323} of tensor (8)

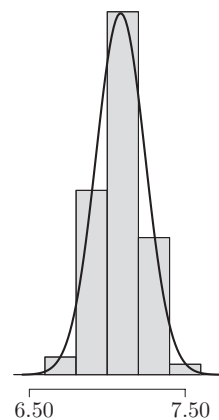


Figure 17: c_{3333} of tensor (8)

6 Discussions and conclusions

The essence of this paper consists of Section 5, in particular, Sections 5.1 and 5.2, therein, as well as Figures 1–6, in which we examine the isotropic counterparts of generally anisotropic elasticity tensors as a function of different norms. Subsequently, we examine consequences of the choice of a norm in reducing a typical tensor obtained from measurements, subject to experimental errors, to its isotropic counterparts. For a general tensor, restricted solely to its stability conditions, the two Frobenius norms result in isotropic counterparts that are sufficiently close to one another that one might neglect their difference within the context of experimental errors. In seismological practice—and perhaps for many naturally occurring materials—one might also ignore the differences between the two Frobenius norms and the operator norm. The similarity of results for the three norms is emphasized

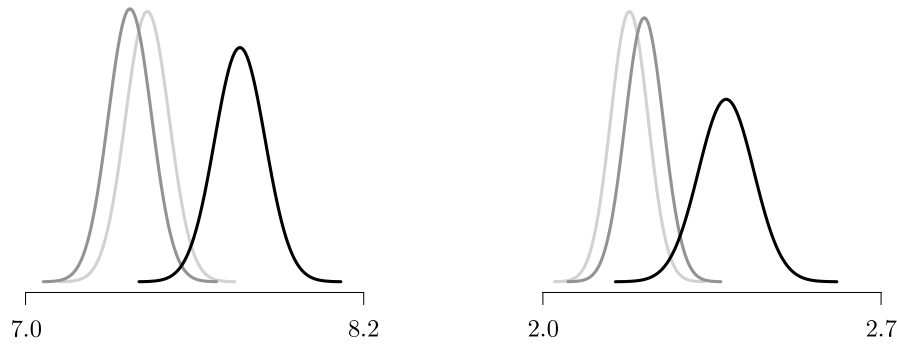


Figure 18: c_{1111} (left panel) and c_{2323} (right panel) of F_{21} (light gray), F_{36} (dark gray) and λ (black) isotropic counterparts of tensor (8)

in Sections 5.3, 5.4 and 5.6, in which—given tensor (8), which represents a typical material—we can find another transversely isotropic tensor representative of common materials such that one of them is closer to isotropy according to one norm and the other one closer to isotropy according to another norm.

Thus, as discussed in Sections 5.1, 5.2, 5.7 and 5.8, the differences among the results of the three norms—and, perhaps, also the slowness-curve fit—might not be crucial within the context of typical materials and measurement errors. Thus, for an important range of Hookean solids, the choice of the norm might be of secondary importance, and, pragmatically, we might choose a Frobenius norm, since it offers analytical formulæ for an isotropic counterpart.

Acknowledgments

We wish to acknowledge the inspiring and fruitful environment of the Dolomites Research Weeks on Approximation in Alba di Canazei where—within the section of Approximations in Seismology—substantial parts of this research were accomplished. Also, we wish to acknowledge discussions with Len Bos, David Dalton, Michael Rochester and Theodore Stanoev, as well as the editorial support of David Dalton and graphical support of Elena Patarini.

This research was performed in the context of The Geomechanics Project supported by Husky Energy. Also, this research was partially supported by the Natural Sciences and Engineering Research Council of Canada, grant 238416-2013, the Polish National Science Center under contract No. DEC-2013/11/B/ST10/0472, and by AGH - University of Science and Technology as a part of the statutory project No. 11.11.140.613.

References

- [1] T. Eken, J. Plomerová, L. Vecsey, V. Babuška, R. Roberts, H. Shomali, and R. Bodvarsson. Effects of seismic anisotropy on P -velocity tomography of the Baltic Shield. *Geophysical Journal International*, 188(2), 2012.
- [2] A. N. Norris. The isotropic material closest to a given anisotropic material. *Journal of Mechanics of Materials and Structures*, 1(2):223–238, 2006.
- [3] L. Bos and M. A. Slawinski. 2-norm effective isotropic Hookean solids. *Journal of Elasticity*, 120(1):1–22, 2015.
- [4] I. Bucataru and M. A. Slawinski. Invariant properties for finding distance in space of elasticity tensors. *Journal of Elasticity*, 94(2):97–114, 2009.
- [5] T. Danek, M. Kochetov, and M. A. Slawinski. Effective elasticity tensors in the context of random errors. *Journal of Elasticity*, 121(1):55–67, 2015.
- [6] T. Danek, M. Kochetov, and M. A. Slawinski. Uncertainty analysis of effective elasticity tensors using quaternion-based global optimization and Monte-Carlo method. *The Quarterly Journal of Mechanics and Applied Mathematics*, 66(2), 2013.
- [7] T. Danek and M. A. Slawinski. On choosing effective elasticity tensors using a Monte-Carlo method. *Acta Geophysica*, 63(1):45–61, 2015.
- [8] T. Danek and M. A. Slawinski. On effective transversely isotropic elasticity tensors of Frobenius and L_2 operator norms. *Dolomites Research Notes on Approximation*, 7, 2014.
- [9] Ç Diner, M. Kochetov, and M. A. Slawinski. On choosing effective symmetry class for elasticity tensors. *The Quarterly Journal of Mechanics and Applied Mathematics*, 64(1):57–74, 2011.
- [10] M. Kochetov and M. A. Slawinski. Estimating effective elasticity tensors from Christoffel equations. *Geophysics*, 74(5):67–73, 2009.
- [11] M. Kochetov and M. A. Slawinski. On obtaining effective orthotropic elasticity tensors. *The Quarterly Journal of Mechanics and Applied Mathematics*, 62:149–166, 2009.
- [12] M. Kochetov and M. A. Slawinski. On obtaining effective transversely isotropic elasticity tensors. *Journal of Elasticity*, 94(1):1–13, 2009.
- [13] M. A. Slawinski. *Waves and rays in seismology: Answers to unasked questions*. World Scientific, 2016.
- [14] D. C. Gazis, I. Tadjbakhsh, and R. A. Toupin. The elastic tensor of given symmetry nearest to an anisotropic elastic tensor. *Acta Crystallographica*, 16:917–922, 1963.
- [15] C. H. Chapman. *Fundamentals of seismic wave propagation*. Cambridge University Press, 2004.
- [16] P. Dewangan and V. Grechka. Inversion of multicomponent, multiazimuth, walkaway VSP data for the stiffness tensor. *Geophysics*, 68(3):1022–1031, 2003.

- 
-
- [17] W. Voigt. *Lehrbuch der Kristallphysics*. Teubner, Leipzig, 1910.
- [18] L. Thomsen. Weak elastic anisotropy. *Geophysics*, 51(10):1954–1966, 1986.
- [19] B. A. Auld. *Acoustic fields and waves in solids*, volume 1. Kreiger Publishing, Florida, 1978.
- [20] J. Guilleminot and C. Soize. On the statistical dependence for the components of random elasticity tensors exhibiting material symmetry properties. *Journal of Elasticity*, 111:109–130, 2013.
- [21] H. Rusmanugroho and G. McMechan. 3D 9C seismic modeling and inversion of Weyburn Field data. *Geophysics*, 77(4):161–173, 2012.